

CPT-BASED CONTROL STRATEGY FOR A TWO-PHASE THREE-WIRE PV INVERTER: A MULTIFUNCTIONAL PERSPECTIVE AND A COMPREHENSIVE REVIEW

Augusto M. S. Alonso^{1*}, João H. Oliveira², Danilo I. Brandao², Jakson P. Bonaldo³, Helmo K. M. Paredes⁴, Fernando P. Marafao⁴

¹University of São Paulo (USP), São Carlos – SP, Brazil

²Federal University of Minas Gerais (UFMG), Belo Horizonte – MG, Brazil

³Federal University of Mato Grosso (UFMT), Cuiabá – MT, Brazil

⁴São Paulo State University (UNESP), Sorocaba – SP, Brazil

e-mail*: augusto.alonso@usp.br

Abstract – Multifunctional inverters play an important role in electrical grids due to their capability to provide active power conversion from photovoltaic (PV) systems, as well as by concomitantly offering ancillary services that provide grid support and power quality improvement. Although control strategies for such inverters have been extensively explored for applications in single- and three-phase grids, their consideration for the two-phase three-wire topology has been superficially discussed in literature. Thus, first, this paper contributes to the literature by presenting a comprehensive review about the control of power electronic inverters in two-phase three-wire grids. As second contribution, this paper proposed a flexible control strategy based on the Conservative Power Theory capable of adequately synthesizing control references for a PV-based multifunctional inverter operating in a two-phase three-wire grid. Additionally, power quality services can be selectively offered by the inverter to achieve compensation of reactive, harmonic and unbalance current terms, as well as providing reduction in neutral currents. Hardware-in-the-loop experimental results comprising a multifunctional PV inverter under several scenarios of operation are shown to demonstrate and validate the flexibility of the method.

Keywords – Ancillary Services, Conservative Power Theory, Power Quality, Two-phase Three-wire.

NOMENCLATURE

A	Apparent power
i_m	m -phase total current
i_{am}^b	m -phase balanced active current
I_a^b	Collective balanced active current
I_{am}^b	m -phase rms balanced active current
i_{am}^u	m -phase unbalanced active current
i_{rm}^b	m -phase balanced reactive current
i_{rm}^u	m -phase unbalanced reactive current
I_r^b	Collective balanced reactive current
I_{rm}^b	m -phase rms balanced reactive current
I^u	Collective unbalanced current
I_m^u	m -phase rms unbalanced current

i_{vm}	m -phase void current
I_v	Collective void current
I_{vm}	m -phase rms void current
i_{pv_m}	MFGTI's active power conversion and DC-link stabilization AC reference current
i_{pv}^{DC}	MFGTI's DC-link current
D	Void power
m	Phase of the $2\Phi 3w$ circuit ($m = a, b$)
N	Unbalance power
P	Active power
P_m	m -phase active power
Q	Reactive power
Q_m	m -phase reactive power
t	Time
T	Period of a voltage or current waveform
v_m	m -phase voltage
V	Collective voltage
V_m	m -phase rms voltage
V_{DC}	MFGTI's DC-link voltage
\hat{v}_m	m -phase unbiased voltage
\hat{V}	Collective unbiased voltage
\hat{V}_m	m -phase rms unbiased voltage
ω_o	Fundamental angular line frequency

I. INTRODUCTION

Multifunctional inverters are key players on the actual energy transition happening world-wide, since they provide means to interface PV-based decentralized power generation in electrical power systems [1]. Beyond their major functionality of ensuring proper power conversion, which means that power generation from PV panels is compliantly integrated to the interconnected grid, such inverters provide ancillary services that can improve their local power quality condition or even support the electrical power system under abnormal circumstances [2]. Thus, by offering additional services and ensuring more flexibility of operation, the concept of multifunctional grid-tied inverters (MFGTIs) rises, representing inverters that use their existing power electronic interfaces to offer ancillary functionalities [3]. For instance, support to functionalities such as reactive power compensation, harmonic and unbalance mitigation, and many others [4], result on the support for a more reliable and robust

Manuscript received 12/21/2021; first revision 02/11/2022; accepted for publication 07/25/2022, by recommendation of Editor Marcelo Lobo Heldwein. <http://dx.doi.org/10.18618/REP.2022.2.0052>

operation of the entire electrical grid, increasing its hosting capacity (e.g., allowing higher PV penetration).

The employment of MFGTIs and their innumerable ancillary functionalities in single- and three-phase low-voltage (LV) grids have been extensively discussed in the literature [2], [4]-[6], also being considered in important standards [7]. Nonetheless, for what concerns the topology of two-phase three-wire ($2\Phi 3w$) grids (i.e., comprised of two phases plus neutral conductor), a limited number of discussions exists due to the particular application of such systems. Electrical grids based on two-phase power are considered to be the first poly-phase systems [8], and the $2\Phi 3w$ topology is still currently found in distribution power systems over the world [9]-[11] (i.e., mostly for residential and rural applications). It is generally an extension of three-phase grids. Moreover, other applications relying on the $2\Phi 3w$ topology are those related to electrical machines [12], power supplies employed on railway traction systems [13], as well as particular scenarios of microgrids [14]. Hence, the adoption of control strategies for MFGTIs under such configuration inherits particularities that are underexplored and need to be addressed and is deemed important to the electrical sector.

Therefore, the following comprehensive literature review is presented aiming at bringing attention to the limited number of researches being developed on the matter of $2\Phi 3w$ topology, mostly concerning the control applications that can be applied to steer power converters in such systems. Concomitantly, such summarization also serves as grounds for the contributions of this paper.

A. Comprehensive Literature Review

Even if limited, three of the aforementioned applications are the ones majorly responsible for driving research on $2\Phi 3w$ power systems. Firstly, microgrid scenarios can be found in literature being based on $2\Phi 3w$ topology [14,15]. In such cases, the grid is devised by two-phases (i.e., with voltages in quadrature) plus neutral conductor, striving for operation under constant power at balanced conditions. Ref. [15] also aims at achieving optimized voltage utilization in comparison to three-phase systems, as well as to consider the direct connection of single and two-phase symmetrical loads (e.g., electrical machines) [14,15]. However, under unbalanced condition, such $2\Phi 3w$ topology cannot be interpreted by conventional three-phase symmetrical components [16], requiring particular analysis of positive and negative sequence components that comprise, for each of them, two phasors of same magnitude but with quadrature angle. Moreover, such existing application requires additional specific understanding of such symmetrical components when harmonic analysis need to be performed [17] under balance and unbalance conditions. In [18], it has also been reassured that off-grid power systems based on $2\Phi 3w$ topology (i.e., such as the above-mentioned particular case of microgrids) require particular interpretation and control approaches, as well as that instantaneous power oscillations and magnitude of neutral current are inversely related.

As second application scenario, railway traction systems also take advantage of $2\Phi 3w$ topology, consequently leading to research on the control of power converters. In [19], a $2\Phi 3w$ quasi-Z-source compensator is employed to devise power

quality improvement in AC rail networks, mainly achieving mitigation of harmonic currents, negative sequence compensation and power factor correction. Another novel converter topology, comprising two step-down transformers, and based on $2\Phi 3w$ configuration, is proposed in [13] for elimination of negative sequence components in railway traction systems, also striving for reduction of power switches ratings. Hysteresis controllers and dividing frequency control is used to drive the converter. In [20] a standalone two-phase voltage inverter with three-legs operating in the overmodulation range is also devised to drive a two-phase motor. Hence, it does not operate connected to a $2\Phi 3w$ grid.

The third application scenario of $2\Phi 3w$ systems is the one related to distribution grids, respectively by the employment of active power filters (APFs) and the exploitation of grid-tied inverters that operate either only interfacing RESs as distributed generators (DGs) or as MFGTIs. With regards to APFs in $2\Phi 3w$, this is the field on which the most significant number of researches is found, even though it is still limited. Control modeling aspects for conventional two-level three-leg inverters in two-phase systems are seldom found in literature. As few examples available, in [21] the small-signal model of a conventional two-level three-leg APF is presented, demonstrating the implementation of its current and voltage control loops, as well as its DC bus voltage controller. In [22], the inner current and outer voltage control loops are also explained, being respectively devised by proportional-resonant (PR) and proportional-integral (PI) controllers. An approach to implement space vector PWM modulation for $2\Phi 3w$ inverters is also shown in [23], reducing the harmonic content and switching losses in such application. Moreover, it has been shown in [24] that the modeling of grid-tied $2\Phi 3w$ inverters can consider model predictive control techniques, integrated with space vector modulation, to obtain fixed switching frequency and good performance upon tracking sinusoidal and non-sinusoidal current references.

When it comes to the generation of control references for APFs in $2\Phi 3w$ power systems, adaptations and particular interpretations of the instantaneous power theory [25], namely $p-q$ theory, have been reasonably explored. For instance, [26] proposes a method on which the single-phase $p-q$ theory has its original axis transformations adapted, being devised by implementation of quadrature filters, resulting in improved instantaneous power calculations that allow to compensate for reactive power and harmonic currents. Such utilization of this alternative single-phase $p-q$ theory is also shown in [11], demonstrating as well that different $2\Phi 3w$ converter topologies can be driven by the approach. In [27], a novel interpretation of the classic $p-q$ theory is devised by mapping two-phase voltages and currents into the $\alpha\beta$ frame by means of linear transformations. Although care must be taken using [28], since the method presents particular interpretations in relation to [29], such approach provides effective reactive power compensation, along with harmonic and unbalance current mitigation, as well as neutral current reduction in $2\Phi 3w$ grids. With the work in [22], another power theory, namely Conservative Power Theory (CPT) [36], has been explored for being applied to the control of APFs in $2\Phi 3w$ networks, achieving selective compensation. Reactive, unbalance and the so-called void current decomposition

provided by the CPT were shown to be effective for compensation purposes.

The concept of analyzing a $2\Phi 3w$ APF by the superposition of two single-phase systems is also presented in [28], taking advantage of the indirect sine multiplying control approach to achieve reduction in neutral currents and regulation of reactive power and harmonic currents. Such approach (i.e., [28]) is also considered for comparisons in [10], showing that effective reduction in neutral currents is obtained, while making the $2\Phi 3w$ power system to see loads as sinusoidal currents sources, as in a conventional phase-to-phase circuit. Other applications of $2\Phi 3w$ APFs propose different converter topologies. For instance, a five-level shunt APF configuration using predictive controllers is devised for compensation of current unbalance and harmonics in [29]. The same topology is employed for reactive power compensation in [30], presenting an innovative DC bus capacitor voltage balancing strategy that requires a reduced number of sensors. In addition, reactive power control, harmonic mitigation, and balancing of currents in $2\Phi 3w$ grids is also presented in [31] and [32] by means of a back-to-back converter that uses predictive directive current control.

Finally, when grid-tied inverters exist in $2\Phi 3w$ grids as interface for renewable energy sources, either as DGs or MFGTIs, very few works have demonstrated in literature how to adequately control their operation. The study within [33] shows that a MFGTI can incorporate the power quality improvement features of the APF in [11], while providing active power conversion from PV-based systems. For such case, a predictive controller is used to generate the switching signals for the inverter, and the compensation of reactive power and current harmonics generated by loads is deemed efficient. Another work [34] focusing on MFGTIs in $2\Phi 3w$ topology demonstrates that active power injection is offered along with reactive power compensation, harmonic current elimination and balancing of currents. Nonetheless, selectivity in control references for compensation purposes is not possible, resulting that the MFGTI does not present flexibility to select the load's unwanted current components. Another work is found in [35], in which a MFGTI is designed as a smarter charger for electric vehicles, concomitantly presenting the capability to compensate for reactive and unbalance currents. Finally, a recent research [37] reinforces the importance of studying PV-based inverters considering the $2\Phi 3w$ topology by discussing reliability concerns behind this particular scenario.

B. Paper Contributions and Organization

Considering the underexplored scenario of $2\Phi 3w$ grids in which a PV-based MFGTI exists along with linear and nonlinear loads, while taking into account the possibility to offer ancillary services aiming at power quality improvement, the contributions of this paper are three-fold:

- This paper brings a survey on the control and application of power inverters focusing on the $2\Phi 3w$ topology, demonstrating that such field should be further studied;
- A flexible strategy is proposed for the control of a MFGTI, being based on concepts within the CPT [36], [38], aiming at providing active power conversion to supply local loads. Additionally, the method supports

power quality improvement by selectively offering: *i*) compensation of reactive currents; *ii*) mitigation of harmonic and unbalance currents; and *iii*) reduction of neutral currents in a $2\Phi 3w$ grid. The proposed approach does not require synchronization algorithms, being devised entirely in the *abc* frame, and it does not cause large voltage oscillations in the DC-link of the MFGTI regardless of the CPT's compensation reference adopted;

- An experimental validation based on hardware-in-the-loop (HIL) results is presented to certify the digital control approach for real applications.

This paper is an extended version of [22], demonstrating the use of the CPT to control a PV-based MFGTI in a $2\Phi 3w$ grid. The dynamics of the DC link control of the inverter considering the power generation intermittency of a PV source is considered, which is also different from [22]. In addition, this paper also brings complementary HIL-based experimental validations to demonstrate the feasibility of the control.

Thus, this paper is organized as follows. Having the background of application given by the literature review in the Introduction section, the CPT power and current terms applied to the $2\Phi 3w$ topology are presented in Section II. Section III presents the flexible control scheme for the operation of the MFGTI, and HIL results in Section IV demonstrate the features of the strategy under several operational scenarios. Finally, conclusions summarize the findings of this paper.

II. THE CPT FRAMEWORK FOR $2\Phi 3w$ APPLICATIONS

Let us consider a $2\Phi 3w$ circuit with periodic quantities, devised as an extension of a traditional three-phase system. Consequently, such circuit is comprised of two conductors that present voltages with 120° phase shift from each other, plus a neutral conductor. As the CPT is entirely defined in the natural-frame reference (i.e., *abc*), herein the subscripts "*a*", "*b*" and "*n*" stand for, respectively, quantities for phases *a*, *b*, and for the neutral wire.

In addition, as a power theory, the CPT decomposes power and current terms based on the conservativeness of the active power (*P*) and reactive energy terms [36]. Such conservative terms are oriented to smart microgrid applications, on which the influence of frequency variations and voltages distortions are required to be analyzed to interpret physical phenomena. However, in this paper, variations in frequency are not considered. Therefore, instead of the reactive energy concept, the reactive power (*Q*) definition is herein considered [37]. For the considered $2\Phi 3w$ topology, the CPT power and current decomposition is defined as follows.

A. Power and Current Decomposition

For the analysis in a $2\Phi 3w$ electrical circuit comprising periodic waveforms with period *T*, *P* is defined by the CPT as given by (1). This active power term is calculated based on the phase voltages, v_m , and the line currents i_m . Herein, the subscript *m* stands for the two phases of the circuit (i.e., $m = a$ or $m = b$). Yet, v_m stands for voltage signals calculated in relation to the neutral conductor "*n*" of the $2\Phi 3w$ circuit. Hence, note from (1) that *P* is attained by summing the mean values of the *m*-phase active powers (P_m) from *a* and *b*.

$$P = \frac{1}{T} \cdot \sum_{m=a,b} \int_0^T v_m \cdot i_m dt = \frac{1}{T} \cdot \int_0^T (v_a \cdot i_a + v_b \cdot i_b) dt. \quad (1)$$

Similarly, the reactive power (Q), which is also a mean value is calculated based on (2) [36]. In this case, the unbiased voltage (\hat{v}_m) shown in (3) is used, considering that ω_o is the fundamental angular line frequency [36]. It is important to reinforce that the CPT's definitions for the reactive, unbalance and harmonic features are different from the ones proposed by Budeanu [39], the IEEE 1549 standard [40], and the classic PQ theory [24]. In addition, each of these power theories present particular interpretations of physical phenomena, requiring extensive discussions to be explained, resulting that comparative analyses are beyond the scope of this paper. Such comparisons and critical evaluations among these power theories are thoroughly discussed in [41] and [42], reinforcing that the aspects related to the CPT are also valid for the $2\Phi 3W$ grid perspective. The scheme in Figure 1 summarizes how some of the most basic terms used on the CPT can be implemented in practical applications. In Figure 1, average (Avg) calculations are performed over the time "t", for instance, by means of moving average filters (MAFs).

$$Q = \frac{1}{T} \cdot \sum_{m=a,b} \int_0^T \hat{v}_m \cdot i_m dt = \frac{1}{T} \cdot \int_0^T (\hat{v}_a \cdot i_a + \hat{v}_b \cdot i_b) dt \quad (2)$$

$$\hat{v}_m = \omega_o \cdot \left(\int_0^t v_m d\tau - \frac{1}{T} \int_0^T v_m dt \right). \quad (3)$$

Now, having P and Q presented, the CPT decomposes current terms that relate to particular physical phenomena existing within the circuit. Given a total m -phase current (i_m) measured at a certain node, the CPT decomposes it in sub-components as shown in (4) and (5), namely active, reactive, and void (distortion) currents, herein defined by the subscripts a , r , and v , respectively. These current components are responsible for, respectively, the active power transfer, the reactive power circulation, and the nonlinearities caused by distortions that are uncommon between voltages and currents. Moreover, the CPT also is able to characterize unbalances (i.e., superscript u) respective to unequal phase conductances (i.e., comprised within the active current parcel) and susceptances (i.e., comprised within the reactive current parcel). Thus, note that the CPT's active and reactive current terms can be further split into the balanced active ($i_{a_m}^b$) and reactive ($i_{r_m}^b$) parcels, as well as the unbalanced active ($i_{a_m}^u$) and reactive parcel ($i_{r_m}^u$).

$$i_m = i_{a_m}^b + i_{r_m}^b + i_{a_m}^u + i_{r_m}^u + i_{v_m} \quad (4)$$

$$i_{v_m} = i_m - (i_{a_m}^b + i_{r_m}^b + i_{a_m}^u + i_{r_m}^u). \quad (5)$$

To obtain such current decomposition defined by the CPT in a $2\Phi 3W$ circuit, the concept of collective value (i.e., bold

variables, V and \hat{V}) is calculated based on the rms value of v_m and \hat{v}_m , as seen in (6) (see also Figure 1.a). It can be seen that, as expected, (7) uses P to calculate the balanced active currents, and Q is similarly used to obtain the balanced reactive current (8). Additionally, as aforementioned, the unbalanced active currents (9) are calculated based on the phase conductances (i.e., obtained by means of P_m and V_m^2) and by considering the equivalent conductance of the circuit. Likewise, the unbalanced reactive currents (10) relate to the respective equivalent and phase susceptances. Note in (7) to (10) that the reactive currents depend on the m -phase unbiased voltages " \hat{v}_m ", instead of the phase voltage " v_m " used for the active current terms.

$$V = \sqrt{V_a^2 + V_b^2}, \quad \hat{V} = \sqrt{\hat{V}_a^2 + \hat{V}_b^2} \quad (6)$$

$$i_{a_m}^b = \frac{P}{V^2} \cdot v_m \quad (7)$$

$$i_{r_m}^b = \frac{Q}{\hat{V}^2} \cdot \hat{v}_m \quad (8)$$

$$i_{a_m}^u = \left(\frac{P_m}{V_m^2} - \frac{P}{V^2} \right) \cdot v_m \quad (9)$$

$$i_{r_m}^u = \left(\frac{Q_m}{\hat{V}_m^2} - \frac{Q}{\hat{V}^2} \right) \cdot \hat{v}_m. \quad (10)$$

One important feature of such current decomposition provided by the CPT, also valid for $2\Phi 3W$ circuits, is that all these decomposed current terms are decoupled, resulting that they can be selectively used for a flexible and independent control of each parcel as desired. Furthermore, since the CPT is devised in the abc frame, such current references are straightforwardly used in time domain, without requiring axis transformations or the use of phase-locked loop (PLL) algorithms, which for instance eliminates issues related to stability [43]. Also, interpretation of such current terms stands as for single- or three-phase systems [44], different from other methods [27]. Another interesting feature of the CPT is related to the fact that, under the operation scenario of non-sinusoidal voltage conditions, compensation of the non-active current terms results in a resistive load synthesis behavior (i.e., the resulting phase currents will be linear to voltage distortions [45]), which can improve the harmonic resonance damping capability of the electric system [46]. Finally, given the collective value of each current term (11) (i.e., respective to (4), see also Figure 1.b), the apparent power (A) is obtained based on the quadratic sum of the active, reactive, unbalance (N) and void (D) (i.e., distortion) power terms, as shown in (12). Such a reconstruction provided by (12) is due to the orthogonality existing among the power terms [36], which is also applied to the case of $2\Phi 3W$ power system. In (12), I is

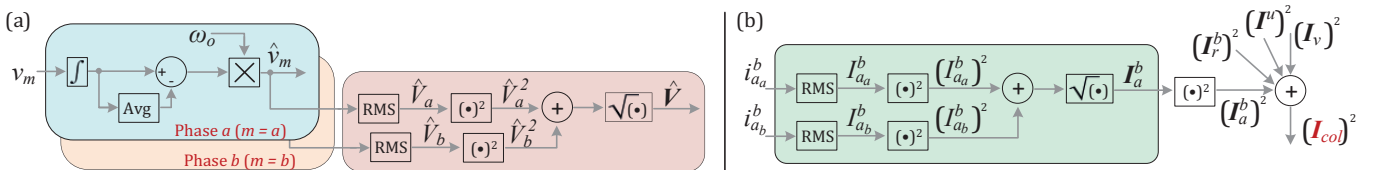


Fig. 1. Calculation of (a) the unbiased and collective voltages, and (b) the total collective current defined by the CPT.

the collective value of the total current, which is equal to I_{col} .

$$I_{col}^2 = (I_a^b)^2 + (I_r^b)^2 + (I^u)^2 + (I_v)^2 \quad (11)$$

$$A^2 = V^2 \cdot I^2 = P^2 + Q^2 + U^2 + D^2 \quad (12)$$

$$N = V \cdot \sqrt{(I_a^u)^2 + (I_r^u)^2} = V \cdot I^u \quad (13)$$

$$D = V \cdot I_v. \quad (14)$$

III. CPT-BASED CONTROL OF A $2\Phi 3W$ MFGTI

To achieve flexible operation regarding operational functionalities, the following control topology presented in Figure 2 is proposed for a three-leg MFGTI existing within a $2\Phi 3W$ power system. Firstly, note that the $2\Phi 3W$ grid is formed as an extension of a conventional three-phase four-wire circuit, comprising line impedances (Z_{line}), and at the point-of-common-coupling (PCC) several loads and a MFGTI are connected. The existing loads are arbitrarily connected to the grid, being also given by linear (i.e., loads $Z_{1,2,\dots,6}$) and nonlinear (i.e., load NL) aggregation of elements, consequently drawing active, reactive, harmonic and unbalance current components. The parameters of such loads are summarized in Table I.

With regards to the MFGTI, a three-leg topology is chosen considering inductive output filters, having the RES placed at the DC bus, consequently allowing the injection of active currents (i.e., being different from [22]). In this paper the inverter is designed to operate under current-controlled mode. Sinusoidal PWM modulation is used to drive the power switches of the inverter.

The control system is devised by two main loops: *i*) one outer voltage loop of slow dynamics, taking advantage of a proportional-integral (PI) controller designed to maintain constant the DC bus voltage (V_{DC}); and *ii*) one inner current loop of fast dynamics that is responsible making the MFGTI current (i_{MFGTI_m}) to track the desired reference ($i_{MFGTI_m}^*$). Proportional-resonant (PR) controllers are usually designed to track the current reference providing zero steady state error [47], but PI current controllers can also be adopted considering the proper disturb compensations, just as done in this paper

and shown in Figure 2. The power conversion from the emulated PV generation system (i.e., resulting in a balanced active current at the AC side of the MFGTI), along with the reference to stabilize the DC-link voltage, are represented by i_{pvm} in Figure 2. The term s_m^* used for the voltage loop is defined to balance the power between the DC and AC sides of the MFGTI as discussed in [22] and [45], being based on the synthesis of sinusoidal currents. In addition, a MAF is used to filter the inherent oscillations existing in the DC-link voltage to achieve better control performance with regards to the mean value of V_{DC} . Yet, note that, since the MFGTI has three legs, only two (i.e., phase *a* and *b* in this case) need to be controlled, being the neutral leg controlled indirectly according to the Kirchhoff's current law. The MFGTI's parameters are shown in Table II.

The flexibility of the control system based on the CPT comes from the "current decomposition block" seen in Figure 2, on which any of the current parcels of the load are extracted and injected by the MFGTI, relieving the grid from supplying them. As seen in Figure 2, the variable "cmd_" is responsible for selecting which of the CPT current parcels will be used on the MFGTI operation (each of the switches commanded by "cmd_" will be triggered according to the discussed intervals of a study case presented in Section IV). This means that the control scheme decomposes the balanced and unbalanced active and reactive currents of the loads, as well as the void current, so that: *i*) the MFGTI can supply the active term as long as power is being generated by the PV-based system; and *ii*) the MFGTI can selectively offer ancillary services for the compensation of reactive power, as well as unbalance and harmonic currents, as long as there is remaining capability available. Moreover, as highlighted in the literature review, these concomitant functionalities under a $2\Phi 3W$ topology are novel since they are devised directly in the *abc* frame by the approach, not relying on PLL algorithms, and being straightforwardly applied to the control system, which provides means to interpret physical electric phenomena without axis transformations.

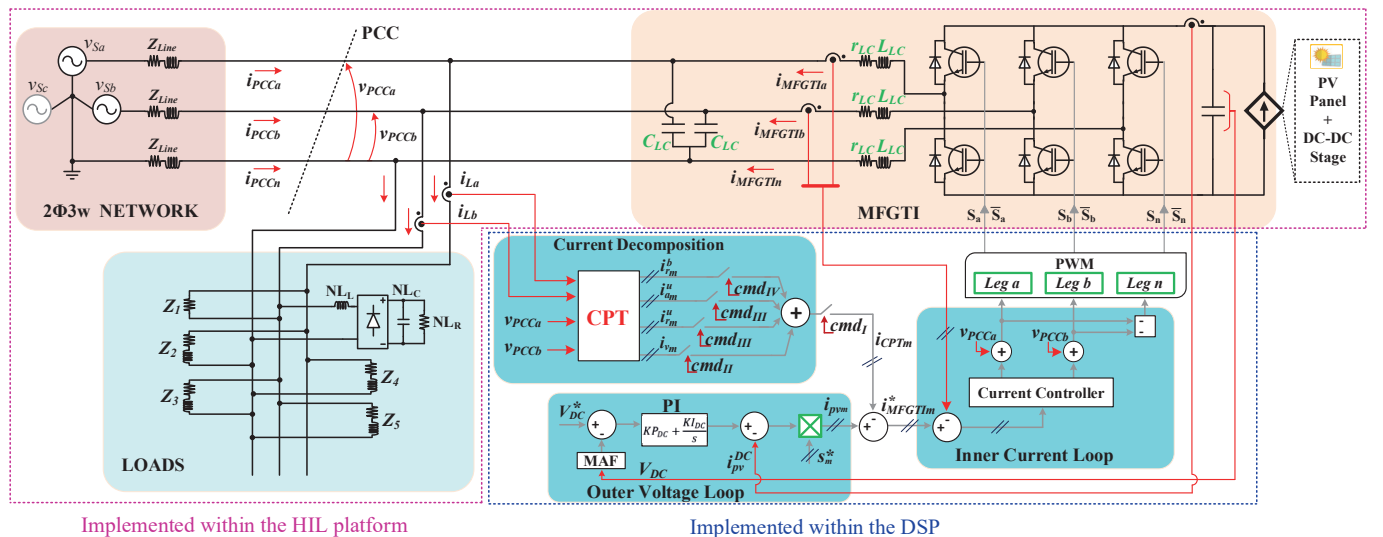


Fig. 2. $2\Phi 3W$ grid and the PV-based MFGTI's electrical and control topologies.

IV. EXPERIMENTAL RESULTS BASED ON HIL

A. Initial Discussions and Setup

Aiming at demonstrating the capabilities of the proposed control approach in a $2\Phi 3w$ power system, HIL results are herein presented considering several operational conditions. The experimental system is comprised of a Typhoon HIL 604, which is used to emulate the entire power system in real time (i.e., the $2\Phi 3w$ grid, the loads, and the power stages of the MFGTI). A host computer is used to interface the HIL platform with MATLAB/Simulink for the programming of such a control board. Hence, all the power circuit elements are built on Simulink, being later embedded to the HIL. On the other hand, the CPT and the control algorithms of the MFGTI (i.e., the voltage and current loops, as well as the PWM approach, both seen in Figure 2) are embedded to a F28069 DSP that is connected to the HIL platform for the complete emulation of the $2\Phi 3w$ circuit. A picture of the experimental setup developed for the assessment of the control strategy is shown in Figure 3.a, and a generic schematic of the input and output connections of the HIL and DSP are shown in Figure 3.b.

A Keysight DSO-X 2014A oscilloscope is used to monitor the AC voltage and current waveforms shown in the results, as well as to attain their instantaneous values, which are later used for calculating the CPT powers used as quantitative indexes. A Rigol MSO7014 oscilloscope monitors the DC-link voltage. It is important to reinforce that the PCC current measurements are only made for phases a and b , being the neutral current calculated by their sum (i.e., $i_{PCCn} = i_{PCCa} + i_{PCCb}$) using an oscilloscope function. Also, although not bringing depreciation to the experimental results obtained, i_{PCCn} could not be inverted (i.e., $i_{PCCn} = -1 \cdot (i_{PCCa} + i_{PCCb})$) due to the limited functionality of the oscilloscope.

The $2\Phi 3w$ power system emulated within the HIL platform considers the grid, load and MFGTI parameters shown in Tables I and II. The parameters used for controlling the MFGTI by means of a C language code embedded into the DSP are also presented in Table II. The PV-based generation system (i.e., PV panel and integrated DC-DC conversion stage) is designed in the HIL system by a controllable DC current source for the sake of simplification. Hence, this current source can emulate any patterns of power generation, similarly to the behavior of a typical PV system. Yet, the CPT powers presented in Section II are also used as quantitative indexes for all simulated cases, demonstrating their suitability for electrical characterization in the $2\Phi 3w$ topology.

Moreover, herein discussions only focus on operation under sinusoidal voltage conditions, although the exact same strategy and experimental setup could be used to demonstrate an adequate operation of the system under non-sinusoidal and/or asymmetrical voltage conditions. It is highlighted that the switching frequency of the MFGTI was chosen to cope with both the typical frequencies adopted for PV inverters, which are around tens of kHz, and the computational requirements of the HIL-based platform. In addition, although the MFGTI was designed considering a nominal power of 25 kVA, the highest apparent power processed during the experiments presented in this section was of around 10 kVA.

B. HIL Results - Study Case

To assess the flexibility of the proposed control approach in the $2\Phi 3w$ topology, a study case is herein presented having

the experimental results divided in five main intervals (i.e., Interval I to V). These five intervals demonstrate, respectively: *i*) The $2\Phi 3w$ grid operating with the nonlinear load and considering the MFGTI acting as an ordinary distributed generator that only injects the PV-generated active power; *ii*) the CPT's current components being used to add ancillary functions to the control strategy of the MFGTI, aiming at mitigating harmonics currents; *iii*) The capability to also compensate for unbalance currents; *iv*) The capability to achieve full compensation of undesired currents at the PCC;

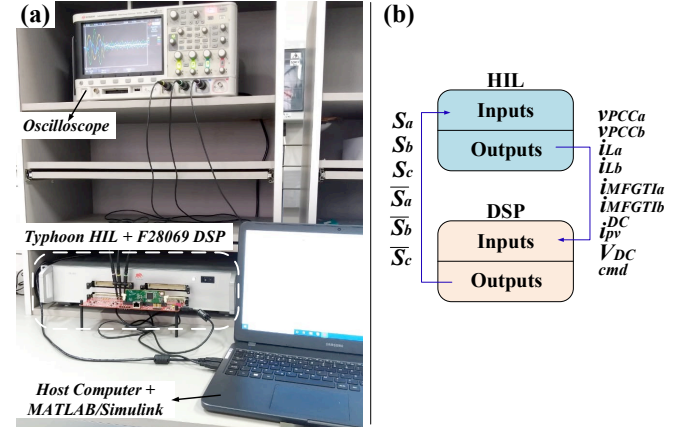


Fig. 3. (a) Setup used for experimental results and (b) inputs/outputs schematic for the integration of the HIL and DSP platforms.

TABLE I
Parameters of the $2\Phi 3w$ Grid With Loads

Parameter	Value
Grid Nominal Voltage: phase-neutral	127 V / 60 Hz
Line Impedances (Z_{line}): per phase	$0.012 + j0.015 \Omega$
Resistive Load (Z_1)	22Ω
Resistive-Inductive Loads (Z_2 and Z_3)	$18 + j4.524 \Omega$
Resistive-Inductive Load (Z_4)	$1 + j6.032 \Omega$
Resistive-Inductive Load (Z_5)	$12 + j4.524 \Omega$
Nonlinear Load (NL)	NL_L 5 mH
	NL_C 470 μ F
	NL_R 10 Ω

TABLE II
Parameters of the $2\Phi 3w$ MFGTI

Parameter	Value	
Nominal Power (A_{MFGTI})	25 kVA	
DC Link Voltage (V_{DC})	500 V	
DC Link Capacitor (C_{DC})	2.5 mF	
Filter Resistance (r_{LC}): per phase	0.095Ω	
Filter Inductance (L_{LC}): per phase	2.5 mH	
Filter Capacitor (C_{LC}): per phase	2.0 μ F	
Switching Frequency (f_{sw})	24 kHz	
Sampling Frequency (f_s)	12 kHz	
Current Controller	Proportional Gain (KP_i)	3.0
	Integral Gain (KI_i)	1.0
Voltage Controller	Proportional Gain (KP_v)	4.0
	Integral Gain (KI_v)	0.0015

and v) the operation dynamics of the MFGTI when an energy generation steps occurs. For all the HIL results comprised within these intervals, the behavior of the MFGTI is mainly verified by demonstrating its processed currents and its DC-link voltage, as well as the impact of its operation at the PCC. The results are discussed as follows.

Initially, Figure 4.a demonstrates during Interval I the results of the study case when the MFGTI operates injecting balanced active currents (i.e., providing power conversion for the PV system), without offering support to ancillary services related to power quality improvement (i.e., “*cmdi*” is open). During this interval, the MFGTI processes 2.4 kW of active power, which represents approximately 35% of the overall active power demanded by the loads. Such an active power injection from the MFGTI is evidenced by its balanced currents (i.e., i_{pv_m}), which are in-phase with the PCC voltages, being also processed with stable operation of the DC-link voltage. At the same time, it can also be seen that the two grid voltages are lagging 120° from each other (i.e., since the $2\Phi 3w$ circuit is derived from a three-phase four-wire power system), as well as that the remaining PCC currents are phase-shifted and distorted (i.e., due to the existence of the loads). For instance, note that the PCC current from phase a (i_{PCCa} – blue curve) is phase-shifted in relation to the voltage of that same phase (v_{PCCa} – orange curve), which indicates the existence of reactive components. Additionally, besides the current unbalance existing between the two phases at the PCC, the currents from phase a and neutral conductor are highly distorted due to the existence of the nonlinear load (see Figure 2). The load unbalance among the phases even causes a small deviation in the amplitudes of the PCC voltages, as noted in Figure 4.a while comparing v_{PCCa} and v_{PCCb} . For instance, the magnitude of phase b voltage is 3% smaller than the one from phase a since most of the loads, including the nonlinear load, are connected between phase b and the neutral conductor. From the behavior of the MFGTI’s DC-link voltage depicted in Figure 4.a, one can note the low-amplitude oscillation with maximum peak-to-peak voltage of 10 V_{dc} (see Table III). Yet, it is evidenced that this voltage is stabilized around 500 V_{dc} (i.e., according to Table II), and a 120 Hz frequency voltage ripple occurs, as expected for this converter topology [37].

As shown in the harmonic decomposition in Figure 5.a, such PCC currents are mainly composed of fundamental terms, also having the 3rd and 5th harmonic orders as the most significant ones. Besides, the total harmonic distortion for PCC phase voltages was THD_{va} = 0.51 % and THD_{vb} = 0.79 %, and for the currents they were THD_i = 2.18 %, 20.6 % and 16.89 %, respectively for phases a , b , and neutral. In Table III the CPT power terms are also presented, characterizing the significant existence of A , P , Q , D , and N power terms. It is reinforced that a significant amount of P is present at the PCC since the injection from the MFGTIs during Interval is not able to fully supply the loads, resulting that there is still active power being drawn from the grid.

Thus, during Interval II in Figure 4.a, the switch commanded by “*cmdi*” is closed (see Figure 2), and the other variables “*cmd_*” are selected in such a way that the MFGTI is enabled to additionally provide the compensation of the CPT void currents (i.e., only “*cmdII*” is closed, resulting that $i_{MFGTI_m}^* = i_{pv_m} + i_{vm}$), which are the distortion currents drawn by the loads. Hence, the MFGTI currents become non-sinusoidal due to the void parcels. Yet, note that the PCC

currents become much less distorted in relation to the Interval I, roughly resembling a sinusoidal shape. This condition is also demonstrated in Table III, on which one can observe a 65% decrease in the distortion power (D) at PCC during Interval II. Moreover, it is evidenced in Figure 4.a that the PCC currents remain notably phase-shifted since reactive components were not mitigated. The THD_i obtained for the PCC currents during Interval II were 1.82%, 2.84%, and 1.91%, respectively for phases a , b , and neutral, which is significantly smaller than during Interval I. Also, the harmonic spectrum shown in Figure 5.b demonstrates that the most significant harmonics have been suppressed by the MFGTI ancillary operation, although the PCC currents were still unbalanced. The DC-link behavior shown in Figure 4.a demonstrates that voltage ripple presented slightly higher amplitude in comparison to Interval I. Such a behavior occurs because the MFGTI needed to process more power to compensate the current harmonics. Nonetheless, the implemented voltage controller was capable to achieve a stable operation during steady state, and no overvoltage occurred neither in the DC nor AC sides of the MFGTI. Finally, it is worth mentioning that, even though the PCC currents visually low distorted, the D term in Table III was not null for several reasons: *i*) the harmonic compensation occurs only up to the bandwidth of the current controller; *ii*) the signal to noise ratio can also affect the measurements due to the ADC resolution; and *iii*) the MFGTI’s LC output filter presents limited filtering capability for high frequency components. In addition, the numerical results from Table III were calculated based on the oscilloscope data, which saves the information with limited resolution.

Now, Figure 4.b starts with a continuation of Interval II, being later changed by Interval III on which the MFGTI is commanded to also provide the compensation of the unbalance current terms (i.e., $i_{MFGTI_m}^* = i_{pv_m} + i_{vm} + i_{am}^u + i_{rm}^u$). Note in Figure 4.b that, by imposing such references for the MFGTI, it rapidly adjusts its operation transiting from Interval II to III, starting to process currents that are distorted and unbalanced in relation to the PCC voltages. As a result, the PCC currents become practically sinusoidal and balanced, proving that the proposed control strategy is able to flexibly provide power quality improvement through the MFGTI. It can be seen from Table III that the unbalance power (N) is practically null in interval III, showing a significant efficiency for the unbalanced current compensation provided by the MFGTI at the PCC. Besides, note in Figure 5.c that the harmonic spectrum is now basically comprised of balanced fundamental components, as a result of having the most significant harmonics and unbalanced components suppressed. Another interesting consequence is that the voltage unbalance previously existing between v_{PCCa} and v_{PCCb} is no longer significant in Interval III. Thus, such a result demonstrates that the selective compensation of current parcels provided by the MFGTI also supports voltage quality improvement. Yet, Figure 4.b shows that again the DC-link operation was stable, presenting a slightly higher voltage ripple in relation to Interval II (i.e., approximately to only 3 V_{dc} higher).

For the fourth scenario of this study case (i.e., Interval IV), the results are shown in Figure 6.a. Initially, the same condition

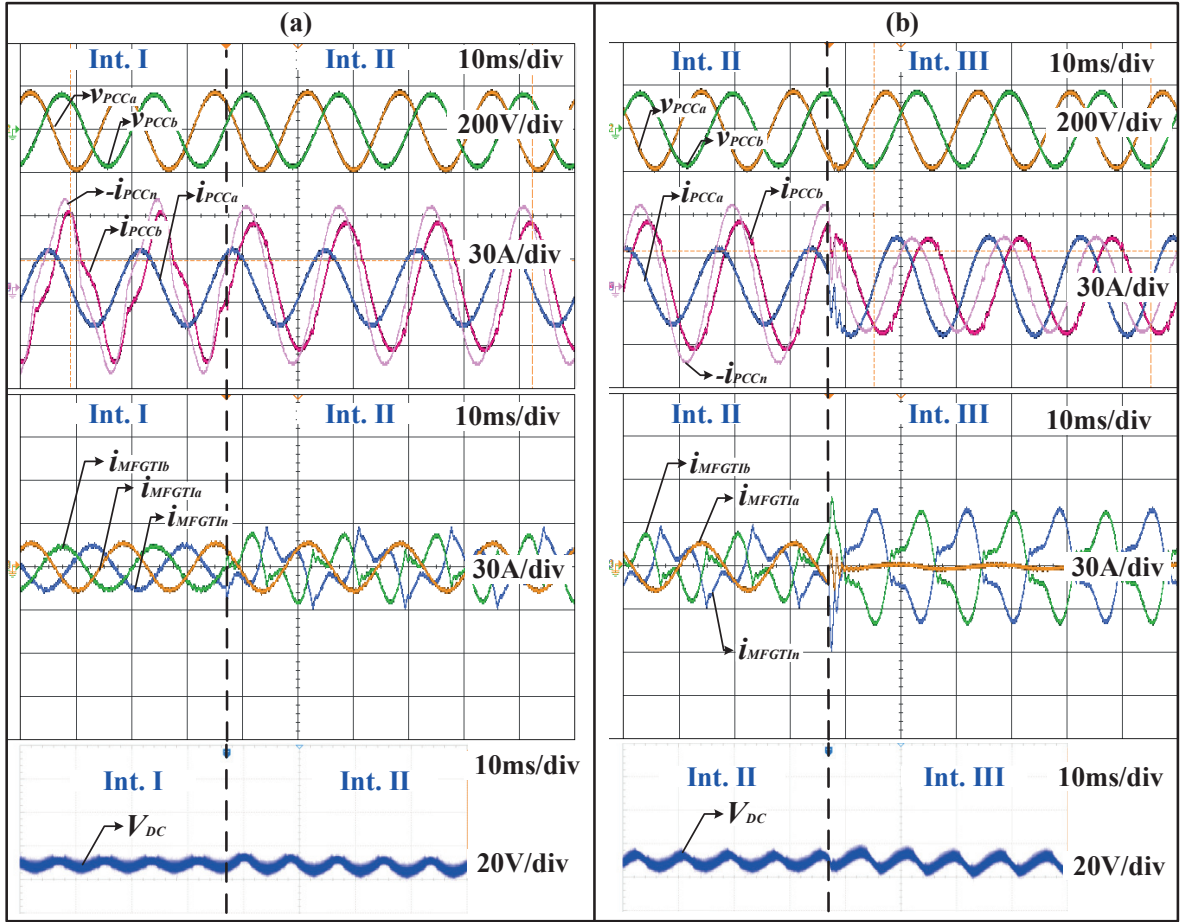


Fig. 4. HIL results for Intervals I, II and III. From top to bottom: PCC voltages and currents, MFGTI currents, and MFGTI DC link voltage. (a) comprises the results for Intervals I and II, starting with the MFGTI only processing 2.4 kW and later i_{vm} is also considered; and (b) shows the transition from Interval II to III, in which the i_m^u is also processed. It is highlighted that the PCC neutral current is presented as $-i_{PCCn}$.

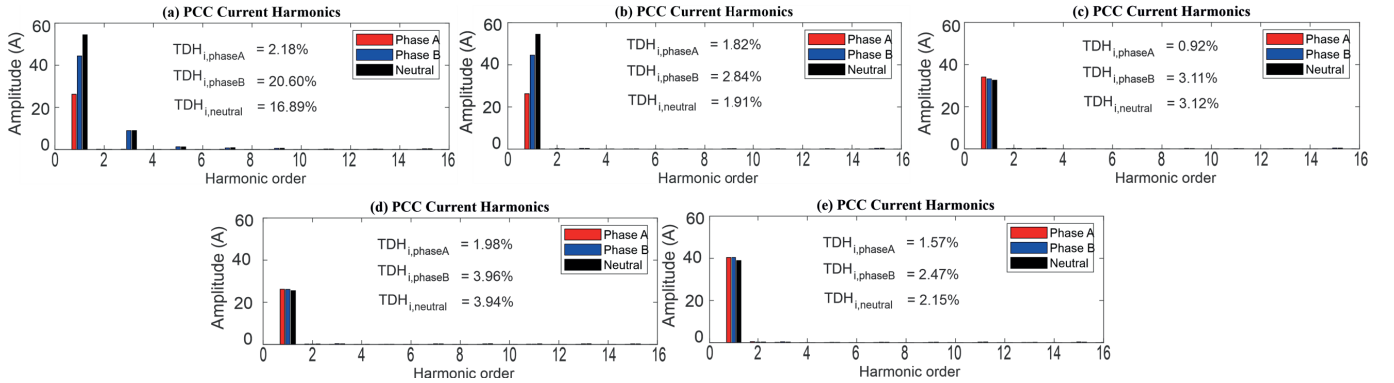


Fig. 5. Amplitude of the PCC currents over the most significant harmonic orders for all intervals in the HIL results: (a) Interval I; (b) Interval II; (c) Interval III; (d) Interval IV; and (e) Interval V.

TABLE III
CPT Powers Calculated at the PCC and Complementary Quantitative Indexes for all Intervals in the Study Case

Quantity		Int. I	Int. II	Int. III	Int. IV	Int. V
CPT Powers	A [VA]	6450.65	6369.09	5891.99	4550.98	7131.85
	P [W]	4186.54	4191.72	4411.49	4543.20	7125.03
	Q [Var]	3907.94	3931.02	3872.92	-118.00	-90.88
	D [VA]	1255.26	429.92	504.07	235.08	245.26
	N [VA]	2696.71	2712.37	25.43	32.56	42.24
PCC Current THD _i [%]	Phase a	2.18	1.82	0.92	1.98	1.57
	Phase b	20.6	2.84	3.11	3.96	2.47
	Neutral	16.89	1.91	3.12	3.94	2.15
MFGTI's Maximum DC-Link		10.10	13.30	16.00	13.00	10.0

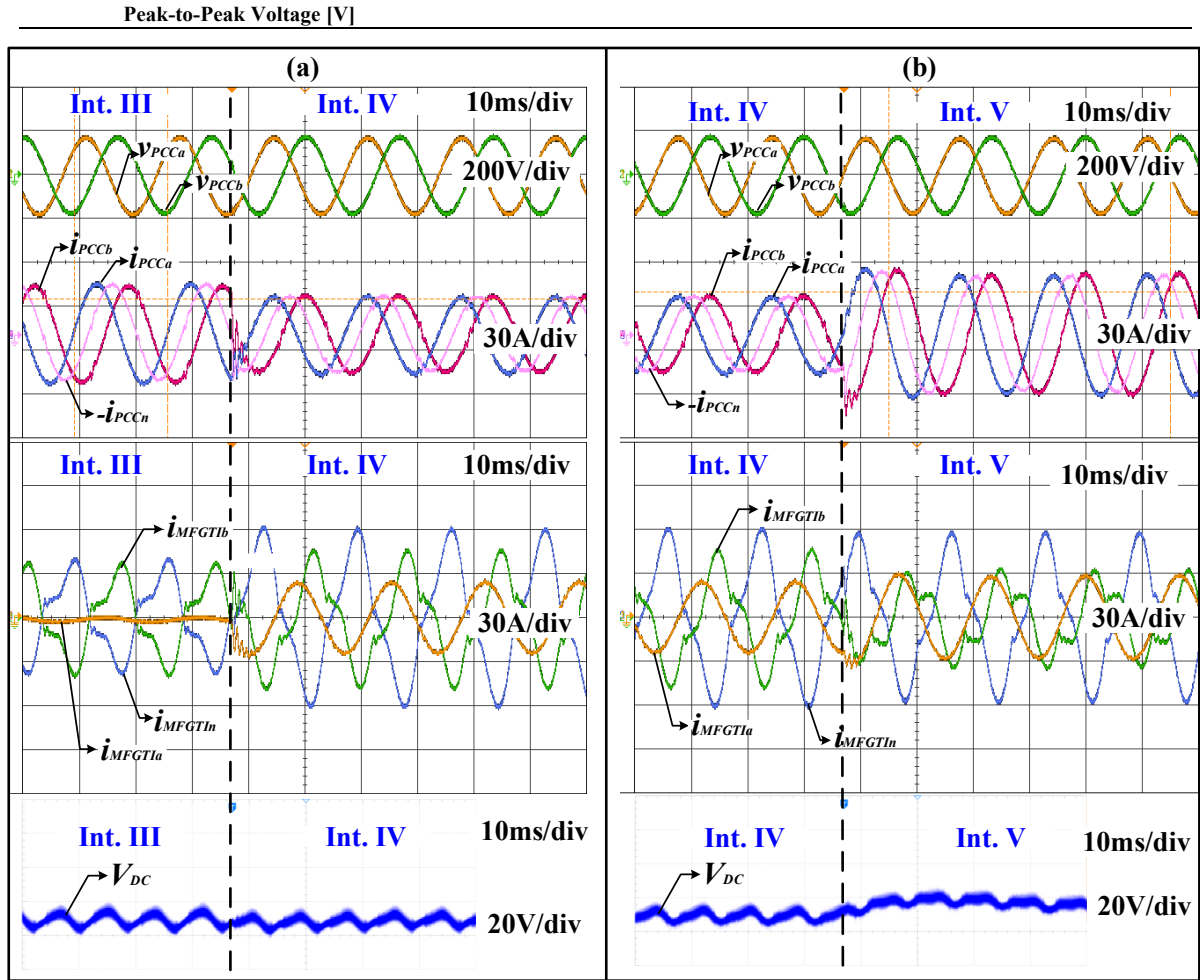


Fig. 6. HIL results for Intervals III, IV and V. From top to bottom: PCC voltages and currents, MFGTI currents, and MFGTI DC link voltage. (a) shows the transition from Interval III to IV, in which the $i_{r_m}^b$ is also processed; and (b) shows the transition from Interval IV to V, in which the PV system suffers a negative step from 2.4 kW to 0 kW. It is highlighted that the PCC neutral current is presented as $-i_{PCCn}$.

from the third scenario (i.e., Interval III) is presented, then the MFGTI current reference is suddenly changed to consider the non-active current parcel along with the active generation from the PV (i.e., $i_{MFGTI_m}^* = i_{pv_m} + i_{r_m}^b + i_{a_m}^u + i_{r_m}^u + i_{v_m}^u$). Note that, the non-active parcel is defined by the CPT as the sum of all unwanted current components drawn by the loads, given that $i_{na_m} = i_{r_m}^b + i_{a_m}^u + i_{r_m}^u + i_{v_m}^u$. Consequently, if the MFGTI is able to supply such currents (i.e., operating as an active filter while also injecting the PV active power), only the balanced active currents would be seen at the PCC. Note in the Interval IV of Figure 6.a that the PCC currents became in-phase with the voltages, being also practically sinusoidal and balanced. The reactive power is supplied exclusively by the MFGTI during this scenario, and Table III shows the effectiveness of the compensation, indicating that the reactive power is practically null. Note in Figure 5.d that the harmonic spectrum is mostly composed by balanced fundamental components, which present smaller amplitudes than those during Interval III.

Finally, a last scenario is demonstrated in Interval V shown in Figure 6.b, on which a negative step for the active power generation is emulated (i.e., the generation is lowered), reducing it to zero similarly to a PV operating at night. Consequently, the MFGTI is not able to supply the active

power demanded by the loads, forcing it to operate as an active power filter. As a consequence, mainly active currents flow through the PCC (note the PCC in-phase and balanced currents in Figure 6.b), and from Table III one can see that P increases during Interval V. This occurs since the MFGTI operates only processing the non-active current terms and the grid takes full responsibility on supplying P to the loads. The harmonic spectrum shown in Figure 5.e also demonstrated that the PCC currents are mainly composed by balanced fundamental components, in a higher amplitude than in Interval IV. As another remark, it is noted in Figure 6-b that the DC-link voltage remains stable during the entire test, presenting a low overshoot when the transitions occur, as well as indicating a lower voltage ripple. For instance, the maximum peak-to-peak value observed for the DC-link voltage during Interval IV is 10 V_{dc}. Finally, Table III demonstrates that the compensation performance of the MFGTI is not affected by the selective operation feature supported by the CPT in the $2\Phi 3w$ power grid, which allows one to determine current parcels to be processed without affecting the others terms.

IV. CONCLUSIONS

This paper presented a comprehensive review about the control of $2\Phi 3w$ power converters, and proposed a flexible control strategy for the operation of PV-based MFGTIs existing in such a grid topology, allowing them to provide ancillary services that can be used to support the power system on tasks related to power quality improvement. With regards to the proposed control strategy, the discussions in this paper have reinforced that the CPT provides an adequate current decomposition to be employed in compensation purposes in $2\Phi 3w$ circuits. Nevertheless, it is worth remarking that the zeroing of the unbalance power term does not mean zero neutral current flowing through the PCC, as it has been presented in Intervals IV and V in Figure 6. Hence, such a feature is most related to the inherent circulation of zero-sequence component even under two balanced phase loads. As another feature, it has also been demonstrated in this paper that by controlling the two phases a and b , while the neutral leg is indirectly controlled according to Kirchhoff's current law, the circuit phases are decoupled, resulting that active, reactive, unbalanced and void (i.e., non-linear distortion) currents can be independently handled.

Finally, experimental results based in HIL validated the proposed control scheme, demonstrating that the method can be adequately implemented in a real digital microprocessor, also proving that the application is valid for the Brazilian scenario (i.e., since $2\Phi 3w$ grids usually operate with 127 V phase voltage and with nominal power lower than 25 kW). The THD values of the compensated PCC currents were about 0-4% as for typical implementations. In addition, the DC-link voltage oscillation varied according to the selective compensation employed, reaching maximum oscillation values of 16 V_{dc} (i.e., about 3.2% of the nominal DC voltage) in the most critical scenario, which was also just 6 V_{dc} higher than when the MFGTI operated only injecting active power. Such an increase in the DC voltage oscillation is also typical of single-phase inverters [6], resulting that the $2\Phi 3w$ inverters do not require any specific sizing of the DC-link capacitor.

ACKNOWLEDGEMENTS

The authors are grateful to FAPESP (Grants 2021/12875-8, 2018/22172-1, 2017/24652-8, 2016/08645-9) and to CNPq (Grant 311332/2018-8).

REFERENCES

- [1] M. H. J. Bollen, and A. Sannino, "Voltage Control With Inverter-Based Distributed Generation," *IEEE Trans. Power Del.*, vol. 20, n° 1, Jan. 2005. DOI: 10.1109/TPWRD.2004.834679
- [2] P. R. M. Costa et al, "Experimental evaluation of a multifunctional system single-stage PV-shunt active filter under partial shading conditions," *Eletrônica de Potência (SOBRAEP)*, vol. 25, n° 2, Jun. 2020. DOI: 10.18618/REP.2020.2.0020
- [3] M. M. Ghahderijani et al, "Imbalance-Voltage Mitigation in an Inverter-Based Distributed Generation System Using a Minimum Current-Based Control Strategy," *IEEE Trans. Power Del.*, vol. 35, n° 3, Jun. 2020. DOI: 10.1109/TPWRD.2019.2945472
- [4] L. V. B. Bellinaso et al, "Strategies to deal with ground faults in grid-connected transformerless photovoltaic converters with battery energy storage system," *Eletrônica de Potência (SOBRAEP)*, vol. 24, n° 3, Sep. 2019. DOI: 10.18618/REP.2019.3.0015
- [5] F. H. M. Rafi et al, "Improved Neutral Current Compensation With a Four-Leg PV Smart VSI in a LV Residential Network," *IEEE Trans. Power Del.*, vol. 32, n° 5, Jun. 2017. DOI: 10.1109/TPWRD.2016.2602220
- [6] D. I. Brandao et al, "Multifunctional Control Strategy for Photovoltaic Distributed Generation Systems," *Eletrônica de Potência (SOBRAEP)*, vol. 18, n° 4, Nov. 2013. DOI: 10.18618/REP.2013.4.12061214
- [7] *IEEE Standard for Interconnection and Interoperability of Distributed Energy Resources with Associated Electric Power Systems Interfaces*, IEEE Standard 1547, 2018.
- [8] T. J. Blalock, "The first polyphase system: a look back at two-phase power for AC distribution," *IEEE Power Energy Mag.*, vol. 2, Aug. 2004. DOI: 10.1109/MPAE.2004.1269626
- [9] J. Viola, M. Fajardo, J. M. Aller, J. Restrepo, F. Quizhpi, "Active Power Filter with Current Balancing Capability for Two-phase Systems," in *Proc. EPE ECCE Europe*, Sep. 2017. DOI: 10.23919/EPE17ECCEEurope.2017.8099252
- [10] P. C. S. Furtado, M. C. B. P. Rodrigues, H. A. C. Braga, P. G. Barbosa, "A Comparison of Two-phase Three-wire Shunt Compensation Strategies," in *Proc. Brazilian Power Electron. Conf.*, Dec. 2015. DOI: 10.1109/COBEP.2015.7420053
- [11] P. C. S. Furtado et al, "Two-phase Three-wire Shunt Active Power Filter Control by Using the Single-Phase P-Q Theory," *Eletrônica de Potência (SOBRAEP)*, vol. 19, n° 3, pp. 303-311, Jun. 2014. DOI: 10.18618/REP.2014.3.303311
- [12] R. E. Fehr, "Industrial Power Distribution", Prentice Hall, 2001.
- [13] C. Wu, A. Luo, J. Shen, F. J. Ma, S. Peng, "A Negative Sequence Compensation Method Based on a Two-Phase Three-Wire Converter for a High-Speed Railway Traction Power Supply System," *IEEE Trans. Power Electron.*, vol. 27, n° 2, pp. 706-718, Feb. 2012. DOI: 10.1109/TPEL.2011.2159273
- [14] E. C. Santos, M. Alibeik, "Microgrid system with voltages in quadrature," in *Proc. IEEE ECCE*, Oct. 2013. DOI: 10.1109/ECCE.2013.6646861
- [15] M. Alibeik, "Different Confiturations of Microgrids and Power Converters," M.Sc. Dissertation, Purdue Univ., July 2014.
- [16] M. Alibeik, E. C. Santos, F. Blaabjerg, "Symmetrical components and power analysis for a two-phase microgrid system," in *Proc. Power and Energy Conf.*, Apr. 2014. DOI: 10.1109/PECI.2014.6804548
- [17] M. Alibeik, E. C. Santos, Y. Yang, X. Wang, F. Blaabjerg, "Harmonic Analysis and Practical Implementation of a Two-phase Microgrid System," in

- Proc. IEEE APEC*, Mar. 2015. DOI: 10.1109/APEC.2015.7104595
- [18] R. M. Silva et al, "Comparison among Two-Phase Three-Wire AC Off-Grid Power Systems," in *Proc. Brazilian Power Electron. Conf. & South. Power Electron. Conf.*, Dec. 2019. DOI: 10.1109/COBEP/SPEC44138.2019.9065785
- [19] H. J. Kaleybar et al, "A Two-Phase Three-Wire Quasi-Z-Source based Railway Power Quality Compensator for AC Rail Networks," in *Proc. IEEE IEEEIC / I&CPS Europe*, Jun. 2017. DOI: 10.1109/IEEEIC.2017.7977713
- [20] D. C. Martins et al, "Two Phase Voltage Inverter with Three Legs Operating in the Overmodulation Range," *Eletrônica de Potência (SOBRAEP)*, vol. 11, Mar. 2006. DOI: 10.18618/REP.2006.1.061068
- [21] M. C. B. P. Rodrigues et al, "Development of a small-signal model for a two-phase three-wire active power filter," in *Proc. Brazilian Power Electron. Conf.*, Nov. 2017. DOI: 10.1109/COBEP.2017.8257255
- [22] A. M. S. Alonso et al, "Selective Power Conditioning in Two-Phase Three-Wire Systems Based on the Conservative Power Theory," in *Proc. IEEE IAS Meeting*, Sep. 2019. DOI: 10.1109/IAS.2019.8911909
- [23] M. Mirazimi et al, "Space vector PWM method for two-phase three-leg inverters," in *Proc. Power Electron. Drive. Syst. Conf.*, Feb. 2016. DOI: 10.1109/PEDSTC.2016.7556920
- [24] P. C. S. Furtado, P. G. Barbosa, "Model Predictive Controller for Two-Phase Three-Wire Grid-Connected Converters," in *Proc. Brazilian Power Electron. Conf. & South. Power Electron. Conf.*, Dec. 2019. DOI: 10.1109/COBEP/SPEC44138.2019.9065666
- [25] H. Akagi, E. H. Watanabe, M. Aredes, "Instantaneous Power Theory and Applications to Power Conditioning," Wiley, Mar. 2017.
- [26] P. C. S. Furtado et al, "Two-phase, Three-wire Shunt Active Power Filter Using the Single-Phase P-Q Theory," in *Proc. Brazilian Power Electron. Conf.*, Oct. 2013. DOI: 10.1109/COBEP.2013.6785275
- [27] P. C. S. Furtado et al, "Adaptation of the Instantaneous Power Theory for Two-phase Three-wire Systems and its Application in Shunt Active Power Filters," in *Proc. Brazilian Power Electron. Conf.*, Dec. 2015. DOI: 10.1109/COBEP.2015.7420017
- [28] P. C. S. Furtado et al, "Shunt Active Compensation Strategy with Zero Neutral Current in Two-phase Three-wire Systems," in *Proc. IEEE Eindhoven PowerTech*, Jun. 2015. DOI: 10.1109/PTC.2015.7232520
- [29] H. Bueno et al, "Shunt active power filter for harmonic compensation of two-phase nonlinear loads," in *Proc. PES T&D Conf.* Sep. 2014. DOI: 10.1109/TDC-LA.2014.6955204
- [30] M. Fajardo et al, "Two-Phase Active Power Filter Direct Current Control with Capacitor Voltages Estimation and Balance," in *Proc. IEEE Workshop Power Electron. Power Quality Appl.*, Jun. 2015. DOI: 10.1109/PEPQA.2015.7168238
- [31] J. Viola et al, "Active Power Filter with Current Balancing Capability for Two-phase Systems," in *Proc. EPE ECCE Europe*, Sep. 2017. DOI: 10.23919/EPE17ECCEEurope.2017.8099252
- [32] J. Viola et al, "Back-to-back active power filter for current balancing in two-phase systems," in *Proc. IEEE Greentech*, Mar. 2017. DOI: 10.1109/GreenTech.2017.26
- [33] P. C. S. Furtado et al, "Topology and control of a two-phase residential PV system with load compensation capability," in *Proc. Int. Symp. Ind. Electron.*, Oct. 2015. DOI: 10.1109/ISIE.2015.7281630
- [34] J. Viola et al, "Grid Connected Inverter with Active Power Filter Capabilities for Two-phase Systems," in *Proc. IEEE 3rd Ecuador Tech. Chap. Meeting*, Oct. 2018. DOI: 10.1109/ETCM.2018.8580259
- [35] T. Tanaka et al, "Smart charger for electric vehicles with power quality compensator on single-phase three-wire distribution feeders," *IEEE Trans. Ind. Appl.*, vol. 49, May 2013. DOI: 10.1109/TIA.2013.2262915
- [36] P. Tenti, H. K. Morales-Paredes, P. Mattavelli, "Conservative Power Theory, a Framework to Approach Control and Accountability Issues in Smart Microgrids," *IEEE Trans. Power Electron.* vol. 26, Mar. 2011. DOI: 10.1109/TPEL.2010.2093153
- [37] J. H. Oliveira et al, "Wear-out prediction of grid-following converters for two-phase three-wire isolated ac power grids," in *Proc. IEEE GreenTech Conf.*, Apr. 2021. DOI: 10.1109/GreenTech48523.2021.00065
- [38] P. Tenti, P. Mattavelli, "A Time Domain Approach to Power Term Definitions under Non-Sinusoidal Conditions," *L'Energia Elettrica*, vol. 81, 2004.
- [39] C. I. Budeanu, "Puissances Reactives et Fictives," *Institute Romain de l'Energie*, n° 2, 1927.
- [40] *IEEE Standard Definitions for the Measurement of Electric Power Quantities under Sinusoidal, Non-sinusoidal, Balanced or Unbalanced Conditions*, 2010, IEEE 1459, Revision of IEEE 1459-2000.
- [41] H. K. M. Paredes, "Teoria de Potência Conservativa: Uma nova abordagem para o controle cooperativo de condicionadores de energia e considerações sobre atribuição de responsabilidades," PhD Thesis, UNICAMP, 2011.
- [42] H. K. M. Paredes et al, "A comparative analysis of FBD, PQ and CPT current decompositions — Part II: Three-phase four-wire systems," in *Proc. IEEE PowerTech*, 2009. DOI: 10.1109/PTC.2009.5282169
- [43] G. Wu et al, "Parameter Design Oriented Analysis of the Current Control Stability of the Weak-Grid-Tied VSC," *IEEE Trans. Power Del.*, vol. PP, Jul. 2020. DOI: 10.1109/TPWRD.2020.3009517
- [44] H. K. M. Paredes et al, "Shunt Active Compensation Based On The Conservative Power Theory," *Eletrônica de Potência (SOBRAEP)*, vol. 17, Feb. 2012. DOI: 10.18618/REP.2012.1.409418
- [45] F. P. Marafao et al, "Multi-task control strategy for grid-tied inverters based on conservative power theory," *IET Renewable Power Generation*, vol. 9, n° 2, pp. 154–165, 2015. DOI: 10.1049/iet-rpg.2014.0065
- [46] A. M. S. Alonso et al, "Resistive Shaping of Interconnected Low-Voltage Microgrids Operating Under Distorted Voltages," *IEEE Transactions on*

Industrial Electronics, 2021. DOI: 10.1109/TIE.2021.3112965

- [47] S. Buso, P. Mattavelli, “Digital Control in Power Electronics”, First edition, Morgan & Claypool, USA, 2006.

BIOGRAPHIES

Augusto M. S. Alonso, received the double Ph.D. degree in electrical engineering in 2021 from the Sao Paulo State University (UNESP), Brazil, and from the Norwegian University of Science and Technology (NTNU), Norway. From January to June 2022 he was a Postdoctoral Researcher funded by FAPESP at the University of Campinas (UNICAMP). Currently, he is an Assistant Professor at the Department of Electrical and Computer Engineering from the University of São Paulo (USP/EESC). In 2015 he was with Whirlpool Latin America/IEL/CNPq as an R&D engineer under the InovaTalentos fellowship. In 2019, he was a recipient of the SOBRAEP award for the best M.S. thesis of the year. His main interests are digital control of power converters, microgrid control, power quality, and energy policies. He is a member of IEEE and SOBRAEP.

João H. Oliveira, born in 09/21/1989 in Timóteo – MG, received the B.S. degree in electrical engineering in 2014 from Federal University of Viçosa (UFV) and the M.S. degree in 2016 from the Federal University of Minas Gerais (UFMG). Currently, he is a PhD student at UFMG. His main interests are control and reliability of power converters, microgrid control and power quality. He is a member of IEEE.

Danilo I. Brandao, received the B.S. degree in control and automation engineering from UNESP, Brazil, in 2011; the M.Sc. degree in electrical engineering from UNESP, Brazil, in 2013; and the Ph.D. degree in electrical engineering from UNICAMP, Brazil, in 2015. He was a visiting scholar at the Colorado School of Mines, USA, in 2009 and 2013, a visiting scholar at the University of Padova, Italy, in 2014, and a guest professor at the Norwegian University of Science and Technology, Norway, in 2018 and 2020. He is currently an assistant professor at the Graduate Program in Electrical Engineering with the Federal University of Minas Gerais (UFMG), Brazil. His main research interests are control of grid-tied converters and microgrids. He is a member of IEEE and SOBRAEP.

Jakson P. Bonaldo, received the B.S. degree in Electrical Engineering from the Federal University of Mato Grosso (UFMT), Cuiabá, Brazil, in 2003. Received the M.S. and the Ph.D. degrees in Electrical Engineering from the University of Campinas (UNICAMP), Campinas, Brazil, in 2010 and 2015, respectively. From 2010 to 2011 he was with Padtec Optical Components and Systems as Firmware Engineer. From 2013-2018 he was with Federal University of Technology - Paraná (UTFPR) as assistant Professor. Since 2018 he is with Department of Electrical Engineering at Federal University of Mato Grosso (UFMT) as assistant professor. His current research interests include power electronics, integration of distributed energy systems and the control of grid-connected power converters. He is a member of SOBRAEP.

Helmo K. Morales-Paredes, received the B.Sc. degree from the National University of San Agustín de Arequipa, Arequipa, Peru, in 2002, and the M.Sc. and Ph.D. degrees from the University of Campinas, Campinas, Brazil, in 2006 and 2011, respectively, all in electrical engineering. In 2009, he joined the Power Electronics Group, University of Padova, Italy, as a Visiting Student. In 2014, he joined the PEMC Group, University of Nottingham, U.K., as a Visiting Scholar. In 2018, he joined the ACEPS Group, Colorado School of Mines, USA, as a Visiting Scholar. Since December 2011, he has been associated with São Paulo State University (UNESP), Sorocaba, Brazil, where he is currently an Associate Professor and the Leader of the Group of Automation and Integrating Systems (GASI). His research interests include power quality, power theories, harmonics propagation, and power electronics applied to renewable energy systems. He is also a member of IEEE, SOBRAEP and SBA. He received the Prize Paper Award from the IEEE TRANSACTIONS ON POWER ELECTRONICS, in 2012.

Fernando P. Marafão, received the B.S. degree in electrical engineering from UNESP, Brazil, in 1998, and the M.Sc. and Ph.D. degrees from UNICAMP, Brazil, in 2000 and 2004, respectively. In 2002, he joined the Power Electronics Group, University of Padova, Italy, as a visiting student. In 2013, he joined the Colorado School of Mines, USA, as a Visiting Scholar. Since 2005, he has been with UNESP, as an Associate Professor with the Group of Automation and Integrating Systems. His current research interests include smart grid technologies, distributed generation, energy management, power electronics and power theories. He is a member of SOBRAEP, SBA and IEEE.